Low-field microwave absorption in epitaxial La$_{0.7}$Sr$_{0.3}$MnO$_3$ films that results from the angle-tuned ferromagnetic resonance in the multidomain state

M. Golosovsky[*] and P. Monod

Laboratoire de Physique du Solide, ESPCI, 10 rue Vauquelin, 75231 Paris Cedex 05, France

P. K. Muduli and R. C. Budhani

Department of Physics, Indian Institute of Technology, Kanpur, 208016, India

We studied magnetic-field-induced microwave absorption in 100–200 nm thick La$_{0.7}$Sr$_{0.3}$MnO$_3$ films on SrTiO$_3$ substrate and found a low-field absorption with a very peculiar angular dependence: it appears only in the oblique field and is absent both in the parallel and in the perpendicular orientations. We demonstrate that this low-field absorption results from the ferromagnetic resonance in the multidomain state (domain-mode resonance). Its unusual angular dependence arises from the interplay between the parallel component of the magnetic field that drives the film into multidomain state and the perpendicular field component that controls the domain width through its effect on domain-wall energy. The low-field microwave absorption in the multidomain state can be a tool to probe domain structure in magnetic films with in-plane magnetization.

I. INTRODUCTION

Low-field microwave absorption is a useful tool of detection of magnetic transitions in bulk materials and thin films.[1–3] It is also known as nonresonant, zero-field, or magnetically modulated microwave absorption and it was used to find the traces of ferromagnetic and superconducting phases in bulk materials.[1,4] The low-field absorption in magnetic materials has multiple sources that operate in different frequency ranges.[5] The dominant contribution at radiofrequencies arises from magnetoimpedance[6–8] (the field dependence of the skin depth) and domain-wall resonances,[9–11] while at microwave frequencies, it is commonly attributed to various ferromagnetic resonances in the magnetically unsaturated state. These include nonaligned ferromagnetic resonance (FMR) mode,[12,13] the natural FMR,[14] off-resonant absorption associated with the FMR tail,[15,16] and the domain-mode resonances.[17–25] Magnetoresistive absorption in conducting ferromagnetics contributes at all frequencies and is most spectacular at the field when magnetization changes abruptly, namely, at zero field[26,27] and upon transition from the unsaturated to saturated state.[28–32]

Manganites are conducting ferromagnetics with exceptionally high magnetoresistance.[33] Their microwave properties in magnetic field have been extensively studied and the low-field microwave absorption was found in many compounds. While the dominant contribution in bulk manganites arises from magnetoimpedance,[14,34] there are many observations of the low-field microwave absorption in thin films that can not be explained in this way. Some of these observations were attributed to magnetoresistance in the magnetically unsaturated state,[8,35,36] while the origin of others[14,32,37,38] is unclear.

Here, we studied microwave absorption in high-quality epitaxial La$_{0.7}$Sr$_{0.3}$MnO$_3$ (LSMO) films in the presence of magnetic field and observed the low-field microwave absorption peak with a very peculiar angular dependence: it appears only in the oblique field. We show that this peak is not related to magnetoresistance but arises from the ferromagnetic resonance in the multidomain state.

II. DOMAIN-MODE RESONANCE IN A THIN FILM WITH "EASY-PLANE" ANISOTROPY IN THE OBLIQUE MAGNETIC FIELD

The theory of the ferromagnetic resonance in the multidomain state was originally developed in relation to bubble or stripe domains in ferromagnetic films with out-of-plane anisotropy.[17,19–21] The few studies of films with in-plane magnetization were restricted to the case of uniaxial anisotropy and parallel field orientation.[18,19] Here, we consider a ferromagnetic film with biaxial easy-plane anisotropy in oblique field and calculate its high-frequency susceptibility following the approach of Refs. 18–20.

A. Magnetostatics

Consider a thin ferromagnetic film in oblique magnetic field H (Fig. 1). Its free energy is

$$W = W_{\parallel} + W_{\perp} + W_{\text{domain}} + W_{\text{Zeeman}} + W(M), \quad (1)$$

where $W_{\parallel}$ and $W_{\perp}$ are the in-plane and out-of-plane anisotropy energies, W_{domain} is the energy associated with domain walls and stray field of domains, W_{Zeeman} is the Zeeman energy, and $W(M)$ absorbs all contributions that do not depend on field orientation. We assume a strong easy-plane anisotropy $W_{\perp} = \frac{N_z M_z^2}{2}$ and a weak in-plane anisotropy $W_{\parallel} = \beta \frac{M_x^4 + M_y^4}{4M^2}$. Here, M is the saturation magnetization, N_z is the effective demagnetizing factor that includes both the shape and the crystalline anisotropies, x, y are hard axes, and β is the (positive) in-plane anisotropy constant, whereas $\beta \ll N_z$. We assume that the external field has only y and z components, in such a way that the field projection on the film plane is parallel to one of the in-plane hard axes.

Figure 1 schematically shows the magnetic structure of the film when the external field slowly decreases to zero. At high field, the film is in the single-domain state, the magnetization lies in the y-z plane [Figs. 1(a) and 1(b)], and $M_x = 0$. At lower field, the magnetization deviates towards the in-plane easy axes (which lie at 45° to x and y axes) and $M_x \neq 0$. The

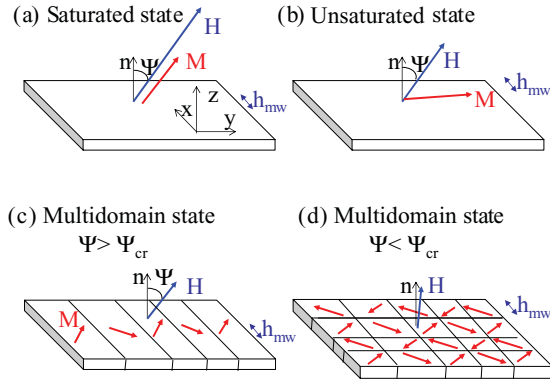FIG. 1. (Color online) Schematic drawing of a thin ferromagnetic film with biaxial easy-plane anisotropy in magnetic field **H** that makes angle Ψ with the normal to the film **n**. **M** is magnetization, $H_\perp$, $H_\parallel$ are the perpendicular and parallel anisotropy fields, hard axes are along the x and y directions. (a) Saturated state. Magnetization is collinear with the field. (b) Unsaturated state. Magnetization is not collinear with the field and tends to lie in the film plane. (c) Multidomain state $\Psi > \Psi_{cr}$. The film is split into parallel domains with the preferential orientation of the walls in the x direction (i.e., perpendicular to H_y). In the presence of a small microwave magnetic field $\mathbf{h}_{mw}$, which is perpendicular to the **H** field and has a component parallel to domain walls, the domain-mode resonance can be excited. (d) Multidomain state $\Psi < \Psi_{cr}$. The resulting domain structure is not clear and we plot only one of the possibilities. The film is split into irregular domains without preferential orientation of the walls, in such a way that the domain-mode resonance is impeded.

film splits onto parallel domains with domain walls in the x-z plane [Fig. 1(c)]. When the field is nearly perpendicular to the film, the resulting magnetic structure is not clear. We believe that the film exhibits an irregular domain pattern [Fig. 1(d)].

Consider the structure shown in Fig. 1(c). Magnetizations of the adjacent domains $\mathbf{M}_1, \mathbf{M}_2$ have the same magnitude but different orientation. The free energy of a domain is

$$W_1 = \beta \frac{M_{1x}^4 + M_{1y}^4}{4M^2} - (M_{1y}H_y + M_{1z}H_z) + \frac{N_z M_{1z}^2}{2}$$
$$+ \frac{N_y(M_{1y} - M_{2y})^2}{4} + \frac{\lambda M^2}{2}, \tag{2}$$

where N_y, N_z are the demagnetizing factors in the y and z directions, $M^2 = M_{1x}^2 + M_{1y}^2 + M_{1z}^2$ is the magnetization, $H_y = H \sin \Psi$, $H_z = H \cos \Psi$ are projections of the field onto y and z axes, and λ is the Lagrange multiplier. The contribution of the domain-wall energy and stray field of domains was neglected. The effective field is

$$\mathbf{H}_1^{\text{eff}} = -\frac{\partial W_1}{\partial \mathbf{M_1}} = -\mathbf{i} M_{1x} \left(\lambda + \frac{\beta M_{1x}^2}{M^2}\right)$$
$$+ \mathbf{j} \left[H_y - \lambda M_{1y} + \frac{\beta M_{1y}^3}{M^2} - \frac{N_y}{2}(M_{1y} - M_{2y})\right]$$
$$+ \mathbf{k}[H_z - (\lambda + N_z)M_{1z}]. \tag{3}$$

A similar expression holds for $\mathbf{H}_2^{\text{eff}}$. The equilibrium condition $\mathbf{H}_1^{\text{eff}} = \mathbf{H}_2^{\text{eff}} = 0$ yields magnetization components

$M_{1y}^{\text{eq}} = M_{2y}^{\text{eq}}$, $M_{1x}^{\text{eq}} = -M_{2x}^{\text{eq}}$, and

$$M_x^{\text{eq}} \left[\lambda + \beta \left(\frac{M_x^{\text{eq}}}{M}\right)^2\right] = 0; \quad M_y^{\text{eq}} \left[\lambda + \beta \left(\frac{M_y^{\text{eq}}}{M}\right)^2\right] = H_y;$$
$$M_z^{\text{eq}}(\lambda + N_z) = H_z, \tag{4}$$

where indices 1, 2 were dropped. The single-domain state corresponds to $M_x^{\text{eq}} = 0$, $\lambda \neq 0$, while the multidomain state corresponds to finite M_x and $\lambda = -\beta(M_x^{\text{eq}}/M)^2$. The onset of the multidomain state occurs when $M_x^{\text{eq}} = 0$ and $\lambda = 0$. Equation (4) yields the field H_0 that corresponds to the onset of the domain state

$$\left(\frac{H_0 \sin \Psi}{H_\parallel}\right)^{\frac{2}{3}} + \left(\frac{H_0 \cos \Psi}{H_\perp}\right)^2 = 1, \tag{5}$$

where $H_\parallel = \beta M$ and $H_\perp = N_z M$ are the parallel and the perpendicular anisotropy fields. For weak in-plane anisotropy $H_\parallel \ll H_\perp$, Eq. (5) yields $H_0 \approx H_\parallel / \sin \Psi$ for $\Psi \gg \Psi_{cr}$, and $H_0 \approx H_\perp$ for $\Psi \ll \Psi_{cr}$ where $\Psi_{cr} = H_\parallel / H_\perp$ is the critical angle that delineates between two regimes that exhibit different domain patterns.

(i) Oblique field $\Psi > \Psi_{cr}$. Upon decreasing field, the film goes from the magnetically saturated to the unsaturated state when the following condition is met: $H \cos \Psi = H_z \approx H_\perp$. At lower field when $H \sin \Psi = H_y = H_\parallel$, the film goes into multidomain state and splits into parallel domains. The preferential direction of the domain walls is determined by the field projection onto the film plane [Fig. 1(c)].

(ii) Nearly perpendicular orientation $\Psi < \Psi_{cr}$. When the film goes from the magnetically saturated to unsaturated state at $H \cos \Psi = H_z \approx H_\perp$, the second condition $H_y = H \sin \Psi \approx H_\parallel$ is already met. The in-plane component of the external field at the onset of the domain state is too small to impose preferential orientation of the domain walls, hence the film most probably splits into irregular domain pattern [Fig. 1(d)].

B. Domain-mode resonance

To derive the dynamic response of the film with parallel domains to the microwave magnetic field $\mathbf{h} = he^{iwt}$ oriented along the domain walls [Fig. 1(c)], we use the Landau-Lifshitz equation without damping

$$\frac{\partial \mathbf{M}}{\partial t} = -\gamma[\mathbf{M} \times \mathbf{H}^{\text{eff}}], \tag{6}$$

where γ is the gyromagnetic ratio. We consider the microwave field as a small perturbation that induces rotation of magnetization of each domain, in other words, we assume $\mathbf{M} = \mathbf{M}^{\text{eq}} + \mathbf{m}$ where $\mathbf{M}^{\text{eq}}$ is the static equilibrium magnetization and $\mathbf{m}$ is a small time-dependent contribution. The effective field also acquires small dynamic contribution $\delta H^{\text{eff}} = \frac{\partial H^{\text{eff}}}{\partial \mathbf{M}} \mathbf{m} + \mathbf{h}_{mw}$, where H^{eff} is given by Eq. (3). We linearize Eqs. (3) and (6) and find the dynamic effective field

$$\delta \mathbf{H}_1^{\text{eff}} = \mathbf{i}(h - \lambda m_{1x}) - \mathbf{j} \left[(\beta + \lambda)m_{1y} + \frac{N_y}{2}(m_{1y} - m_{2y})\right]$$
$$- \mathbf{k}(\lambda + N_z)m_{1z}. \tag{7}$$

A similar expression holds for domain 2. Solution of Eqs. (6) and (7) yields two eigenfrequencies

$$\omega_l^2 = \gamma^2 M_x^2 \beta \left(N_z \frac{5M_y^2 - M_x^2}{M^2} + \beta \frac{6M_z^2 M_y^2 - 2M_z^2 M_x^2 - 5M_y^2 M_x^2 + M_x^4}{M^4} \right), \quad (8)$$

$$\omega_h^2 = \gamma^2 M_x^2 \left[N_y N_z + \beta \left(N_y \frac{4M_z^2 - M_x^2}{M^2} + N_z \frac{5M_y^2 - M_x^2}{M^2} + \beta \frac{6M_z^2 M_y^2 - 2M_z^2 M_x^2 - 5M_y^2 M_x^2 + M_x^4}{M^4} \right) \right]. \quad (9)$$

Since magnetization in the unsaturated state is almost parallel to the film, we can simplify these cumbersome expressions by omitting the terms with M_z. Equations (8) and (9) reduce to

$$\omega_l^2 \approx \gamma^2 M_x^2 \beta \left(N_z - \frac{\beta M_x^2}{M^2} \right) \left(\frac{5M_y^2 - M_x^2}{M^2} \right), \quad (10)$$

$$\omega_h^2 \approx \gamma^2 M_x^2 N_y \left(N_z - \frac{\beta M_x^2}{M^2} \right). \quad (11)$$

Both eigenfrequencies depend on external field (through M_x) and go to zero at the onset of the domain state where $M_x = 0$. The lower frequency ω_l almost does not depend on the domain structure since in this "acoustic" mode the magnetizations of neighboring domains precess almost in phase. On the other hand, the higher frequency ω_h depends on the domain shape (through the demagnetizing factor N_y) since in this "optical" mode the magnetizations of neighboring domains precess in antiphase and the resulting magnetization has poles on the domain walls. The complex susceptibility

$$\chi_{xx} = \frac{m_{1x} + m_{2x}}{2h} \approx \frac{\gamma^2 M_y^2 \left(N_z - \frac{\beta M_x^2}{M^2} \right)}{\omega_h^2 - \omega^2} \quad (12)$$

exhibits resonance at $\omega = \omega_h$. The resonant frequency can be crudely estimated from Eq. (11):

$$\omega_h \sim \gamma M_x \sqrt{N_y N_z}. \quad (13)$$

Since the domain demagnetizing factors are $N_z \approx \frac{w}{d+w}$, $N_y \approx \frac{d}{d+w}$ where d is the film thickness and w is the domain width,[18] Eq. (13) yields $\omega_h \approx \gamma M_x \frac{\sqrt{wd}}{w+d}$ (we neglected here the contribution of stress and crystallographic anisotropy to N_z). When the field is decreased to zero, the magnetization in domains rotates (affecting M_x), domain width w also changes, in such a way that ω_h and, correspondingly, the microwave susceptibility [Eq. (12)] can pass through the resonance. For nearly perpendicular field orientation, when the film splits into irregular domains [Fig. 1(d)], such resonance is impeded.

Although the above model assumes that the field projection on the film plane is exactly along the hard magnetization axis (Fig. 1), this assumption is probably not too restrictive. To observe the domain-mode resonance, it is necessary to have a system of parallel domains with alternating magnetizations and the component of the microwave magnetic field parallel
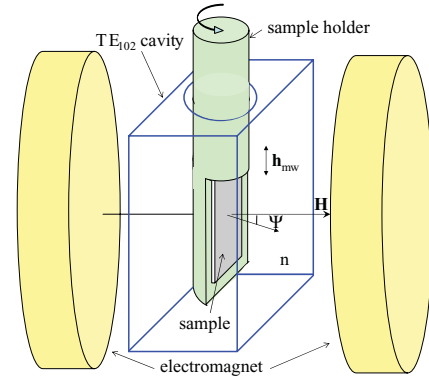

FIG. 2. (Color online) Schematic drawing of the sample in magnetic field. A sample holder with attached film on substrate is mounted in the center of the 9.4-GHz TE_{102} resonant cavity. The polar angle of the magnetic field **H** is varied by sample rotation. The microwave magnetic field $\mathbf{h}_{mw}$ is always perpendicular to **H** and parallel to the film plane.

to the domain walls. This requirement can be satisfied when the field projection on the film considerably deviates from the hard magnetization axis, especially for the films with biaxial in-plane anisotropy.

III. EXPERIMENT AND COMPARISON TO MODEL

A. Experimental procedure

To measure the low-field microwave absorption associated with the domain-mode resonance, we used a bipolar
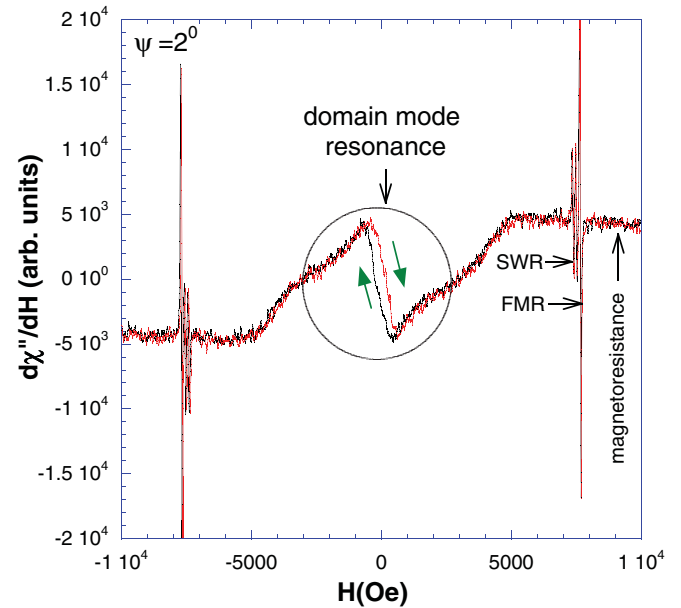

FIG. 3. (Color online) Derivative microwave absorption for a 200-nm-thick LSMO film on (001) STO substrate in magnetic field deviating from the perpendicular orientation by $\Psi = 2°$. The ferromagnetic (FMR) and the spin-wave resonances (SWR) appear at ± 7.6 kOe, and the absorption baseline results from magnetoresistance. Note strong zero-field feature between -2 and 2 kOe that shows considerable hysteresis. We attribute it to the domain-mode resonance.

X-band Bruker ESR spectrometer, a TE_{102} resonant cavity, and an Oxford helium flow cryostat (Fig. 2). We studied La$_{0.7}$Sr$_{0.3}$MnO$_3$ films with thicknesses $d = 50$, 100, 150, and 200 nm. The films were grown by the pulsed laser deposition technique on the $\sim 5 \times 5 \times 1$ mm^3 (001) SrTiO$_3$ substrates in two different laboratories[39,40] and have T_C of 330 K. The FMR measurements in the parallel field showed biaxial (fourfold) in-plane anisotropy of all these epitaxial films. We measured magnetically modulated microwave absorption and dispersion in 1×1 mm^2 pieces of these films when the magnetic field was swept from large negative to large positive values (typically, from -10 to 10 kOe). To change the field orientation with respect to the film, we rotated the sample whereas the microwave magnetic field was always parallel to the film plane and perpendicular to the dc magnetic field. To find the exact perpendicular orientation, we slightly tilted the sample holder in different directions, measured the field of the ferromagnetic resonance, and found the orientation in which the resonant field attained its maximum value. In what follows, we focus on the results for the different pieces of the 200-nm-thick film. We got similar results for the 100- and 150-nm-thick films, but not for the 50-nm-thick film. According to our interpretation, this difference can be related to the different domain structure in thin films, the thickness of which is comparable to the domain-wall width.

B. Low-field microwave absorption at 295 K

Figure 3 shows derivative microwave absorption in oblique field for the 200-nm-thick film and for two opposite directions of the field sweep. The narrow peaks at ± 7.6 kOe arise from the ferromagnetic and spin-wave resonances, the baseline arises from magnetoresistance, and the pronounced zero-field feature exhibiting hysteresis is attributed to domain-mode resonance. This zero-field feature does not depend on the magnitude (1–10 Oe) or frequency of the modulation field (1–100 kHz).

Figure 4 shows corresponding integrated absorption χ'' and dispersion χ' (details of the integration procedure are in Ref. 36). The absorption baseline linearly increasing with field arises from magnetoresistance (rigorously speaking, from magnetoconductance) and is absent in the dispersion spectrum, as expected. The focus of our study is a low-field peak in the absorption spectrum and a corresponding dip in the dispersion spectrum. We attribute both these features to the tail of the domain-mode resonance. Indeed, we substitute into Eq. (13) $w = 0.5$ μm,[41,42] $d = 200$ nm, $4\pi M_x = 4\pi M = 4$ kG and find $\omega_h/2\pi = 5.1$ GHz. This value is below but not far away from our operating frequency of 9.4 GHz, hence the tail of the resonance should introduce positive contribution to χ'' and negative contribution to χ' [Eq. (12), $\omega_h < \omega$] that conforms to our observations (Fig. 4).

Note that the magnitude of the zero-field absorption peak is close to the magnitude of the FMR peak. Since the FMR
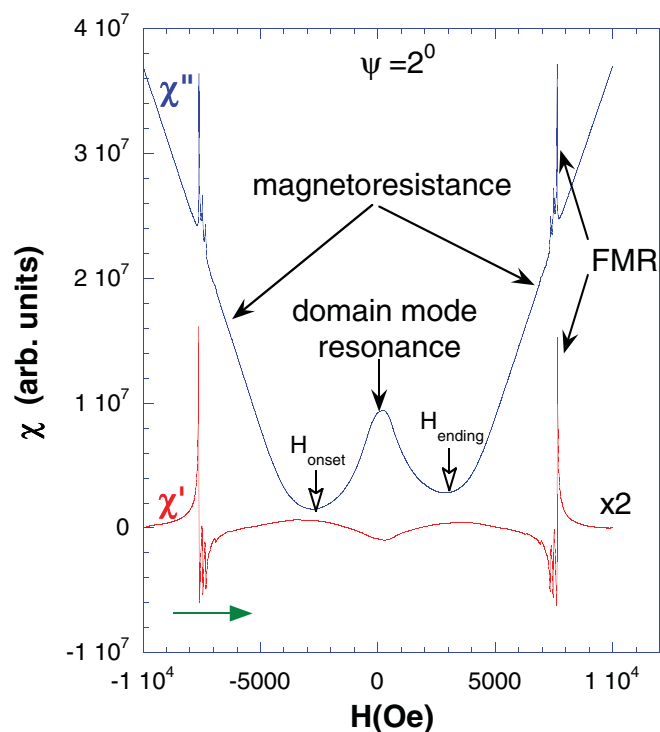

FIG. 4. (Color online) Integrated microwave absorption χ'' and dispersion χ' for the film shown in Fig. 3. The linear baseline in the absorption spectrum results from magnetoresistance, while the zero-field peak and the corresponding zero-field dip in the dispersion spectrum are attributed to the domain-mode resonance. H_{onset} and H_{ending} indicate the field range where the low-field absorption appears.
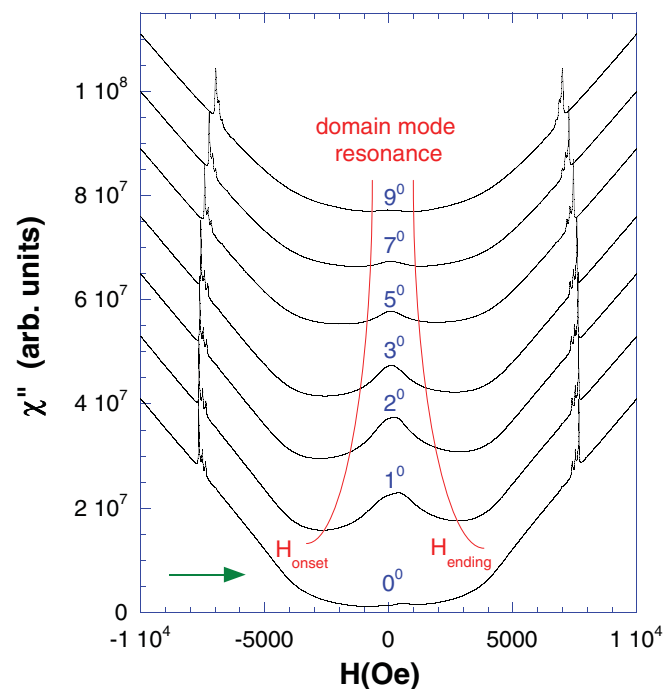

FIG. 5. (Color online) Integrated microwave absorption at different deviations of the field from the perpendicular orientation. The low-field absorption peak appears in the narrow angular range of $8° > |\Psi| > 1°$ close to the perpendicular orientation. The red dashed line shows the field interval where this low-field absorption appears. This interval narrows with increasing Ψ. The field corresponding to the maximum absorption also shifts with the angle and depends on the direction of the field sweep. The curves are vertically shifted for clarity.
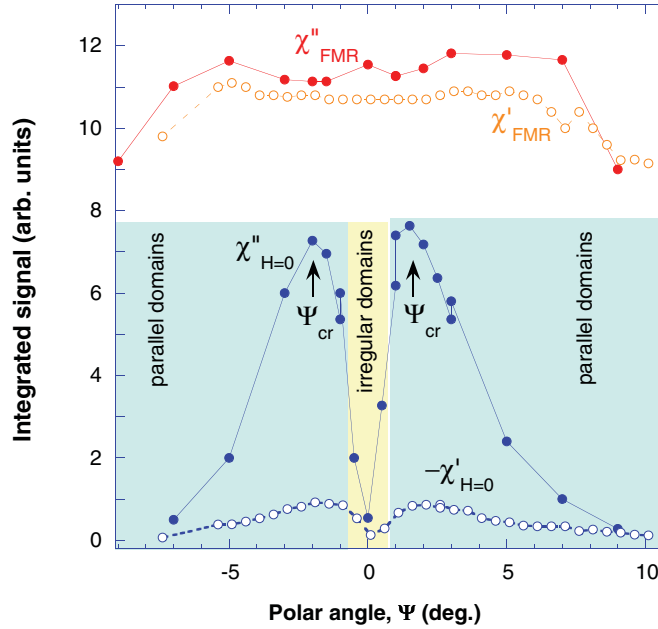
FIG. 6. (Color online) Angular dependence of the microwave susceptibility at zero field $\chi''_{H=0}$, $\chi'_{H=0}$ and at the ferromagnetic resonance χ''_{FMR}, χ'_{FMR} (peak-to-peak). The filled circles stay for absorption, the open circles stay for dispersion. The low-field absorption peak appears only at some deviation from the perpendicular orientation when the parallel domains are expected (gray area). The absorption peak disappears when the deviation from the perpendicular orientation is less than $1°$ (yellow area) when the domain pattern is, presumably, irregular.

absorption peak arises from the microwave absorption in the whole film, the zero-field absorption peak is an intrinsic effect (if it were related to the microwave absorption associated with some defect, its magnitude should be much smaller). Moreover, when we took a film with the size 5×5 mm^2 and cut it to several smaller pieces, we observed the zero-field absorption peak in each piece.

1. Angular dependence

Figure 5 shows that the low-field absorption peak appears in the oblique field and disappears when the field deviation from the perpendicular orientation is too large or too small. Since the conventional protocol of the angular-dependent microwave absorption measurements with the ESR spectrometer starts from $\Psi = 0°$ and goes with $10°$ steps, it is not a surprise that the low-field absorption peak with such a peculiar angular dependence was overlooked in previous studies.

Figure 6 shows angular dependence of the maximum low-field absorption and dispersion χ'_{max}, χ''_{max}, as well as the magnitude of the FMR peak χ'_{FMR}, χ''_{FMR}. In the narrow angular range around perpendicular orientation, the latter are nearly constant, while the former appear at $|\Psi| < 8°$, grow towards perpendicular orientation, and suddenly disappear in the even more narrow angular range of $|\Psi| < 1°$.

2. Field dependence

The low-field absorption achieves its maximum value χ'_{max} at small but nonzero field H_{center}, which depends on
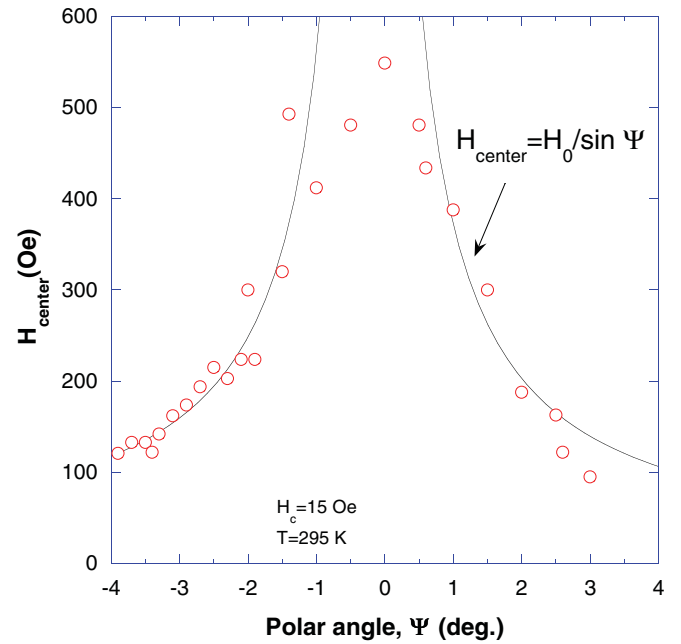

FIG. 7. (Color online) The field at which the maximum zero-field absorption appears at $T = 295$ K. The solid lines show approximation by the following dependence: $H_{center} = H_0/\sin\Psi$, where Ψ is the polar angle and $H_0 = 7.8$ Oe.

the direction of the field sweep (Fig. 3) and on the field orientation (Fig. 7). The angular dependence of this field is satisfactorily accounted by the following function $H_{center} \approx H_0/\sin\Psi$ where $H_0 = 7.8$ Oe, which is close to the coercive field. This means that the maximum absorption is achieved when the in-plane component of the magnetic field is close to the coercive field that is consistent with Eq. (13) (since $M_x \approx M$ at $H_y = H_c$, then ω_h most closely approaches ω).

Figure 8 shows the field range where the low-field absorption peak is observed at 295 K. This range has a four-lobed shape with the lobes oriented along the directions $|\Psi| = 2.6°$. Remarkably, this value coincides with the critical angle that was defined in relation to Eq. (5). Indeed, by substituting into Eq. (5) the perpendicular anisotropy field $H_\perp = 4$ kOe (measured from the FMR in the perpendicular geometry), and the parallel anisotropy field $H_\parallel = 180$ Oe (found from magnetization measurements), we find $\Psi_{cr} = H_\parallel/H_\perp = 2.6°$. The lobes are within the rectangle defined by the conditions $H_y < H_\parallel$, $H_z < 0.7H_\perp$. The former defines the onset of the multidomain state for the nearly parallel field orientation, while the latter means that the magnetization lies predominantly in-plane (more precisely, the deviation of the magnetization from the in-plane orientation does not exceed $45°$).

3. Comparison to the model

The unusual angular dependence of the low-field absorption peak (Fig. 6) and its hysteretic behavior (Fig. 3) imply that the peak magnitude strongly depends on the field orientation during magnetic field sweep. How can such dependence on magnetic history be qualitatively explained by Eqs. (11) and (12)? The film has out-of-plane hard axis in the z direction
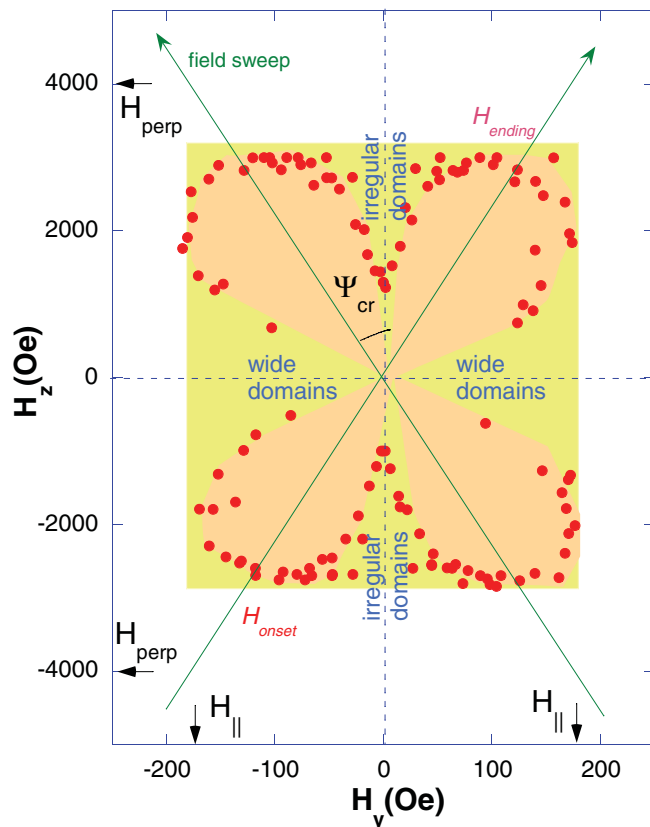
FIG. 8. (Color online) The range of magnetic fields where the low-field microwave absorption peak appears. The red circles stand for the onset and the ending fields at which the low-field absorption peak is observed upon the field sweep from −10 to 10 kOe (see Fig. 5). Note different horizontal and vertical scales. $H_\perp$ and $H_\parallel$ stand for the perpendicular and parallel anisotropy fields. The yellow rectangle indicates the field range where domain structure can appear. The brown area enclosed by the data points shows the field range where the low-field microwave absorption appears.

and the in-plane hard axes in the x and y directions. Figure 8 shows that the low-field absorption appears when the film is in the unsaturated state both with respect to the out-of-plane and in-plane hard axes. This state is presumably the multidomain state. Indeed, there are quite a few observations of magnetic domains in the LSMO films on STO.[41,43–47] Photoelectron emission spectroscopy[46] revealed (3–30)-μm wide parallel domains, magnetic force microscopy showed much smaller, 1-μm-wide domains,[47] or the checkerboard domain pattern with (0.5–0.75)-μm wide domains,[41] and even smaller 0.3-μm-wide domains (in LCMO thin films).[42] To explain our results, we assume parallel domains, the width and orientation of which depend on the values of H_z and H_y at the onset of the domain state, hence the dependence on magnetic history.

We attribute the absorption peaks shown in Figs. 4 and 5 to the tail of the domain-mode resonance. The peak magnitude is set by the proximity of the resonant frequency ω_h to the operating frequency ω. Dependence of ω_h on magnetic history is captured by the parameter N_y [Eq. (13)], which is determined by the domain width w. The latter is found by minimizing the sum of the energy associated with the stray field of domains

and the total energy of domain walls W_{DW}.[48] The onset of the multidomain state is set by H_y, while the domain-wall energy and, correspondingly, the domain width are set by H_z. The latter can strongly affect the energy and structure of the domain walls and even drive the transition from the Bloch to Néel wall.[48,49] When the field is lowered, the domain width changes, but due to pinning, some memory of the magnetic conditions at the onset of the multidomain state is conserved. Since H_y and H_z play very different roles in establishing the domain state, the domain pattern and the frequency of the domain-mode resonance [Eq. (13)] depend on field orientation during field sweep, hence the resulting absorption peak is strongly angular and field dependent. We can speak on "angle-tuned" domain-mode resonance.

When the field is parallel to the film, domain width is large and ω_h is too low to produce appreciable absorption at $\omega/2\pi = 9.4$ GHz. When the field is close to the perpendicular orientation, the domain width is small, ω_h approaches ω, and absorption strongly increases. When the field is too close to the perpendicular orientation, there is no preferential domain-wall orientation, domain pattern is irregular, and the resonance is not excited. These considerations can be succinctly summarized as follows: $H_z \rightarrow W_{DW} \rightarrow w \rightarrow N_y \rightarrow \omega_h \rightarrow \chi_{max}$.

C. Low-field microwave absorption at low temperatures

Table I demonstrates that the maximum low-field absorption χ''_{max} (achieved at different angles for each temperature) does not disappear at low temperatures and even increases. This stays in sharp contrast with the microwave losses associated with magnetoconductance (magnetoresistance), the magnitude of which, for our highly conducting films, dramatically decreases at low temperatures. This proves once again that the low-field microwave absorption is unrelated to magnetoresistance. We observe also that χ''_{max} is on the same order as the FMR absorption peak in the parallel geometry. This is not surprising since according to our model, the zero-field absorption peak is nothing else but the FMR absorption peak in the parallel geometry, which is shifted to zero field due to dynamic demagnetization factor associated with magnetic domains.

The temperature dependence of the low-field absorption is dictated mostly by ω_h and its proximity to the operating frequency ω [Eq. (13)]. The low-field absorption at 295 K

TABLE I. Comparison of different contributions to microwave absorption. (The units are arbitrary, but the same for all entries.)

T (K)	$\chi''_{H=0}$ [a]	χ''_{FMR} [b]	χ''_{MR} [c]
295	3.3	2.5	31
270	3	1	12
220	2.5	3.4	6.2
110	4.3	4	2.8
4.5	8.8	2.6	<0.3

[a]The maximum low-field microwave absorption (at corresponding angle).

[b]The magnitude of the FMR absorption peak in parallel field.

[c]Nonresonant microwave losses associated with magnetoresistance in parallel field $\chi''_{MR} = \chi''_{H=10\,kOe} - \chi''_{H=0}$.
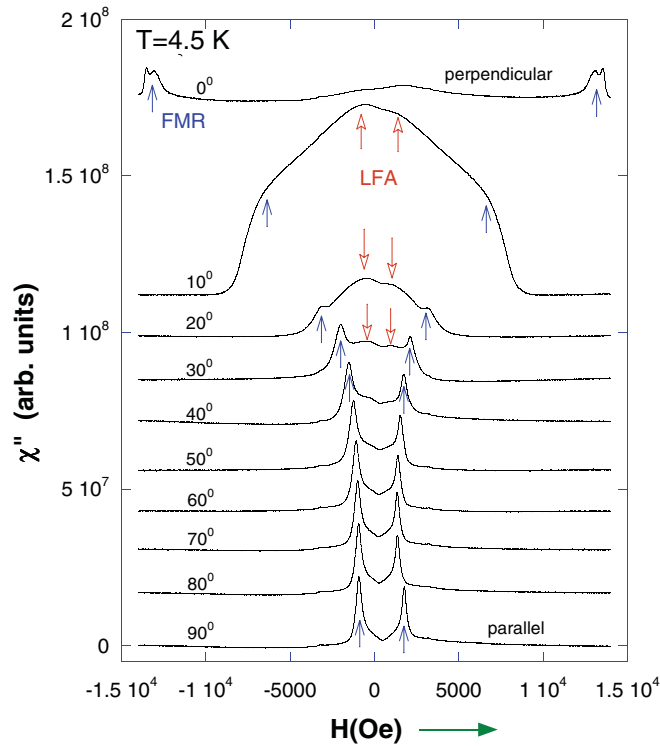
FIG. 9. (Color online) Integrated absorption for the sample of Fig. 5 at 4.5 K at different field orientations. The blue arrows indicate some of the FMR peaks, and the red arrows indicate low-field absorption peaks associated with the domain-mode resonance. The FMR peaks appear in all orientations, while the domain-mode resonance appears only in oblique orientation and disappears both in the parallel and perpendicular orientations. Unlike Fig. 5 where at each field orientation there is a single low-field absorption peak, here there are two overlapping peaks.

arises from the tail of the domain-mode resonance since $\omega_h < \omega$. To estimate ω_h at 4.5 K, we note that at 4.5 K, $4\pi M =$

7.4 kG (saturation magnetization of LSMO). We substitute this value, $d = 200$ nm, $w = 0.5$ μm into Eq. (13) and find $\omega_h/2\pi = 12.2$ GHz, in such a way that $\omega_h > \omega$. This means that the maximum absorption is achieved at resonant field that satisfies the condition $\omega_h = \omega$. Upon field sweep across the zero, this condition is met twice: once for negative and once for positive field.

Figure 9 shows the low-temperature microwave absorption spectra at different angles. In contrast to Fig. 5, there are two low-field absorption peaks: one at negative and one at positive field. There are other differences with respect to Fig. 5 as well. The baseline in Fig. 9 is flat, indicating negligible contribution from magnetoresistance, in such a way that in the parallel orientation, the absorption spectrum exhibits only the FMR peak. When the field is rotated away from the parallel orientation, there appears a low-field absorption peak that becomes a dominant feature at $\Psi = 5°$–$20°$. This peak disappears again when the deviation from the perpendicular orientation is less than $1°$.

IV. CONCLUSIONS

In thin $La_{0.7}Sr_{0.3}MnO_3$ films with easy-plane anisotropy, there is a special kind of the domain-mode resonance that is absent in the parallel and perpendicular field orientation and appears only in the oblique magnetic field. It can be angle tuned by varying the field orientation with respect to the film. The resonance in oblique field should not be unique to manganites, and it can be a source of pronounced low-field microwave absorption in other magnetic materials as well.

*Permanent address: The Racah Institute of Physics, the Hebrew University of Jerusalem, 91904 Jerusalem, Israel; michael.golosovsky@mail.huji.ac.il

[1]R. C. Haddon, S. H. Glarum, S. V. Chichester, A. P. Ramirez, and N. M. Zimmerman, Phys. Rev. B **43**, 2642 (1991).

[2]B. F. Kim, J. Bohandy, K. Moorjani, and F. J. Adrian, J. Appl. Phys. **63**, 2029 (1988).

[3]F. J. Owens, J. Phys. Chem. Solids **58**, 1311 (1997); **66**, 793 (2005).

[4]A. I. Veinger, A. G. Zabrodskii, and T. V. Tisnek, Supercond. Sci. Technol. **8**, 368 (1995).

[5]G. F. Dionne, IEEE Trans. Magn. **39**, 3121 (2003).

[6]R. Valenzuela, R. Zamorano, G. Alvarez, M. P. Gutierrez, and H. Montiel, J. Non-Cryst. Solids **353**, 768 (2007).

[7]H. Montiel, G. Alvarez, R. Zamorano, and R. Valenzuela, J. Non-Cryst. Solids **353**, 908 (2007).

[8]D. Stanescu, P. Xavier, J. Richard, and C. Dubourdieu, J. Appl. Phys. **99**, 073707 (2006).

[9]N. Bahlmann, R. Gerhardt, and H. Doetsch, J. Magn. Magn. Mater. **161**, 22 (1996).

[10]V. T. Synogach and H. Dotsch, Phys. Rev. B **54**, 15266 (1996).

[11]N. Vukadinovic, J. Ben Youssef, H. Le Gall, and J. Ostorero, Phys. Rev. B **62**, 9021 (2000).

[12]G. A. Prinz, G. T. Rado, and J. J. Krebs, J. Appl. Phys. **53**, 2089 (1982).

[13]F. Gerhardter, Yi Li, and K. Baberschke, Phys. Rev. B **47**, 11204 (1993).

[14]S. E. Lofland, V. Ray, P. H. Kim, S. M. Bhagat, K. Ghosh, R. L. Greene, S. G. Karabashev, D. A. Shulyatev, A. A. Arsenov, and Y. Mukovskii, J. Phys.: Condens. Matter **9**, L633 (1997).

[15]S. J. Lee, C. C. Tsai, H. Cho, M. Seo, T. Eom, W. Nam, Y. P. Lee, and J. B. Ketterson, J. Appl. Phys. **106**, 063922 (2009).

[16]M. Rivoire and G. Suran, J. Appl. Phys. **78**, 1899 (1995).

[17]J. O. Artman, Phys. Rev. B **105**, 74 (1957).

[18]T. E. Hasty, J. Appl. Phys. **35**, 1434 (1964).

[19]N. M. Salansky and B. P. Khrustalev, Czech. J. Phys. **21**, 419 (1971).

[20]N. A. Buznikov and K. N. Rozanov, J. Magn. Magn. Mater. **285**, 314 (2005).

[21]A. Layadi, F. W. Ciarallo, and J. O. Artman, IEEE Trans. Magn. Mag- **23**, 3642 (1987).

[22]N. Vukadinovic, J. Ben Youssef, and H. Le Gall, J. Magn. Magn. Mater. **150**, 213 (1995).

[23]U. Ebels, P. E. Wigen, and K. Ounadjela, J. Magn. Magn. Mater. **177**, 1239 (1998).

[24]S.-Y. Bi, J. Appl. Phys. **67**, 3179 (1990).

[25]O. Acher, C. Boscher, B. Brule, G. Perrin, N. Vukadinovic, G. Suran, and H. Joisten, J. Appl. Phys. **81**, 4057 (1997).

[26]A. A. Zakhidov, I. I. Khairullin, V. Y. Sokolov, R. H. Baughman, Z. Iqbal, M. Maxfield, and B. L. Ramakrishna, Synth. Met. **43**, 3717 (1991).

[27]J. Dubowik, F. Stobiecki, and P. Y. Goscianska, Czech. J. Phys. **52**, 227 (2002).

[28]K. Fukui, K. Uno, H. Ohya-Nishiguchi, and H. Kamada, J. Appl. Phys. **83**, 2158 (1998).

[29]J. J. Krebs, P. Lubitz, A. Chaiken, and G. A. Prinz, J. Appl. Phys. **69**, 4795 (1991).

[30]F. J. Rachford, P. Lubitz, and C. Vittoria, J. Appl. Phys. **53**, 8940 (1982).

[31]B. A. Belyaev, A. V. Izotov, and A. L. Leksikov, IEEE Sensors Journal **5**, 260 (2005).

[32]V. V. Demidov, I. V. Borisenko, A. A. Klimov, G. A. Ovsyannikov, A. M. Petrzhik, and S. A. Nikitov, J. Exp. Theor. Phys. **112**, 825 (2011).

[33]M. B. Salamon and M. Jaime, Rev. Mod. Phys. **73**, 583 (2001).

[34]S. Budak, M. Ozdemir, and B. Aktas, Phys. B (Amsterdam) **339**, 45 (2003).

[35]D. L. Lyfar, S. M. Ryabchenko, V. N. Krivoruchko, S. I. Khartsev, and A. M. Grishin, Phys. Rev. B **69**, 100409(R) (2004).

[36]M. Golosovsky, P. Monod, P. K. Muduli, R. C. Budhani, L. Mechin, and P. Perna, Phys. Rev. B **76**, 184414 (2007).

[37]M. Golosovsky, M. Abu-Teir, D. Davidov, O. Arnache, P. Monod, N. Bontemps, and R. C. Budhani, J. Appl. Phys. **98**, 084902 (2005).

[38]D. K. Aswal, A. Singh, R. M. Kadam, M. K. Bhide, A. G. Page, S. Bhattacharya, S. K. Gupta, J. V. Yakhmi, and V. C. Sahni, Mater. Lett. **59**, 728 (2005).

[39]K. Senapati and R. C. Budhani, Phys. Rev. B **71**, 224507 (2005).

[40]F. Yang, L. Mechin, J. M. Routoure, B. Guillet, and R. A. Chakalov, J. Appl. Phys. **99**, 024903 (2006).

[41]E. P. Houwman, G. Maris, G. M. De Luca, N. Niermann, G. Rijnders, D. H. A. Blank, and S. Speller, Phys. Rev. B **77**, 184412 (2008).

[42]S. J. Lloyd, N. D. Mathur, J. C. Loudon, and P. A. Midgley, Phys. Rev. B **64**, 172407 (2001).

[43]P. Lecoeur, Pl. Touilloud, Gang Xiao, A. Gupta, G. Q. Gong, and X. W. Li, J. Appl. Phys. **82**, 3934 (1997).

[44]J. Dho, Y. N. Kim, Y. S. Hwang, J. C. Kim, and N. H. Hur, Appl. Phys. Lett. **82**, 1434 (2003).

[45]Y. Murakami, H. Kasai, J. J. Kim, S. Mamishin, D. Shindo, S. Mori, and A. Tonomura, Nat. Nanotechnol. **5**, 37 (2010).

[46]T. Taniuchi *et al*., Appl. Phys. Lett. **89**, 112505 (2006).

[47]M. Ziese, Phys. Status Solidi B **243**, 1383 (2006).

[48]A. Hubert and R. Schaefer, *Magnetic Domains. The Analysis of Magnetic Microstructures* (Springer, Berlin, 1998), p. 238.

[49]S. A. Manuilov, A. M. Grishin, and M. Munakata, J. Appl. Phys. **109**, 083926 (2011).